Supplementary Information (SI) for Nanoscale.
This journal is © The Royal Society of Chemistry 2025

Realizing Zero-Threshold Population Inversion via Plasmonic Doping -Supplementary Information

Mohsin Ijaz,[1,2,3,*] Hao Zhang,[1,2,3,*] Isabella Wagner,[1,2,4] Fengjiang Liu,[5,6] Margarita Samoli,[7,8] Zeger Hens,[7,8] Pieter Geiregat,[7,8] Justin M. Hodgkiss,[1,2,4] Richard J. Blaikie,[1,2,3] Boyang Ding,[1,2,3] Yu-Hui Chen,[9,†] Kai Chen,[1,2,10,‡] and Min Qiu[5,6,§]

[1] *Dodd-Walls Centre for Photonic and Quantum Technologies, New Zealand*
[2] *MacDiarmid Institute for Advanced Materials and Nanotechnology, New Zealand*
[3] *Department of Physics, University of Otago, PO Box 56, Dunedin 9016, New Zealand*
[4] *School of Chemical and Physical Sciences, Victoria University of Wellington, Wellington 6012, New Zealand*
[5] *Key Laboratory of 3D Micro/Nano Fabrication and Characterization of Zhejiang Province, School of Engineering, Westlake University, 18 Shilongshan Road, Hangzhou 310024, Zhejiang Province, China*
[6] *Institute of Advanced Technology, Westlake Institute for Advanced Study, 18 Shilongshan Road, Hangzhou 310024, Zhejiang Province, China*
[7] *Physics and Chemistry of Nanostructures, Ghent University, 9000 Ghent, Belgium*
[8] *Center for Nano and Biophotonics (NB Photonics), Ghent University, 9000 Ghent, Belgium*
[9] *Key Laboratory of advanced optoelectronic quantum architecture and measurements of Ministry of Education, Beijing Key Laboratory of Nanophotonics & Ultrafine Optoelectronic Systems, School of Physics, Beijing Institute of Technology, Beijing 10081, China*
[10] *Robinson Research Institute, Victoria University of Wellington, Lower Hutt 5010, New Zealand*

(Dated: January 6, 2025)

* These authors contributed equally
† stephen.chen@bit.edu.cn
‡ kai.chen@vuw.ac.nz
§ qiu_lab@westlake.edu.cn

CONTENTS:

1. **Sample fabrication and structures**

2. **Optical measurement setups**

3. **Dispersive optical properties of the plasmonic resonator**

4. **Determine the resonant enhancement of absorption**

5. **Transient Photoluminescence at different pump powers**

6. **Transition assignment**

7. **Estimation of excited carriers**

8. **Hot electrons in plasmonic resonators**

9. **Modified Emission via plasmonic doping**

I. SAMPLE FABRICATION AND STRUCTURES

The process of fabricating large-area silver (Ag) gratings on a cm^2 scale involved the use of Lloyd's-mirror-interference lithography and pattern-transfer techniques as described in reference [1]. The surface topography of the gratings was evaluated using Atomic Force Microscopy (AFM, Nanosurf NaioAFM). As depicted in Fig. S1**a**, the Ag grating had a period of 500 nm and a groove depth of 100 nm. Spin coating of CdSe/CdS (core/shell) quantum dots (QDs) with an outer diameter of ~ 7 nm and core diameter of ~ 4 nm onto the Ag grating caused the groove depth to decrease to ~ 20 nm, as illustrated in Fig. S1**b**. This implies that the QDs filled the space between Ag lines. Based on the AFM measurements in Fig. S1**c**, we can estimate that the coverage of QDs on the quartz surface results in a thickness of ~ 45 nm, which forms a 6 – 7 layer film. It is noteworthy that the QDs utilized in this study are the same as those used in our prior research works [2, 3].

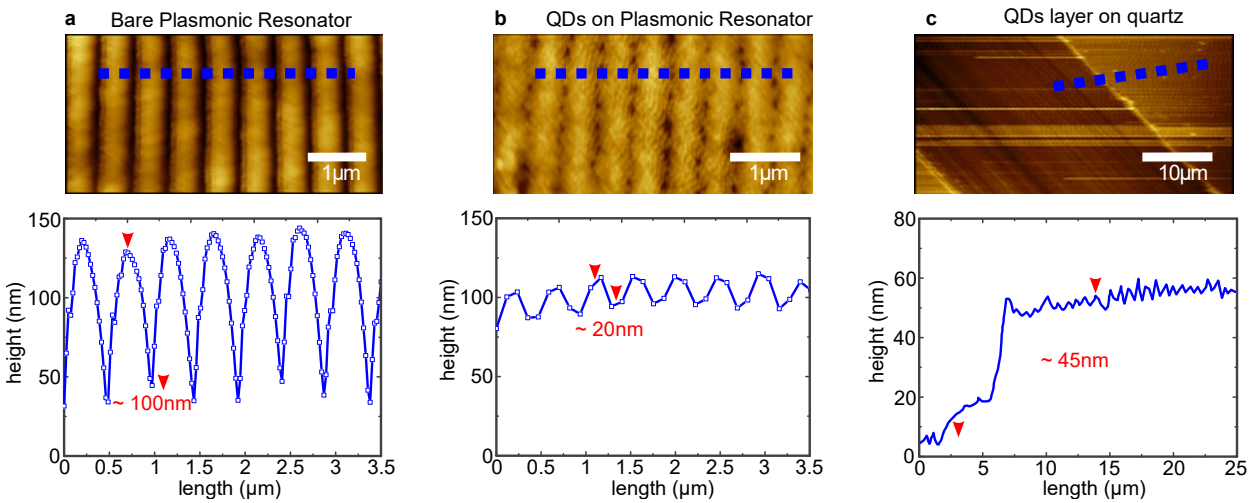

Fig. S 1. **AFM characterizations of: a,** bare Ag grating, **b,** Ag grating coated with QDs at 3000 rpm, and **c,** QDs layer deposited on quartz at 3000 rpm. Bottom panels are AFM data measured at the position marked respectively by the blue dashed lines, and the while bars indicate the scales as noted.

As noted in the main text, we also prepared a reference sample with a dielectric spacer that separated the QD layers from the metal surface. To achieve this, we spin-coated a Poly-Vinyl-Alcohol (PVA) layer with a thickness of approximately 20 nm on the Ag grating before depositing the QDs on top. The bare QD samples of the spacer-embedded hybrid reference were prepared by coating a glass substrate with the PVA layer and then depositing the QDs on top.

II. OPTICAL MEASUREMENT SETUPS

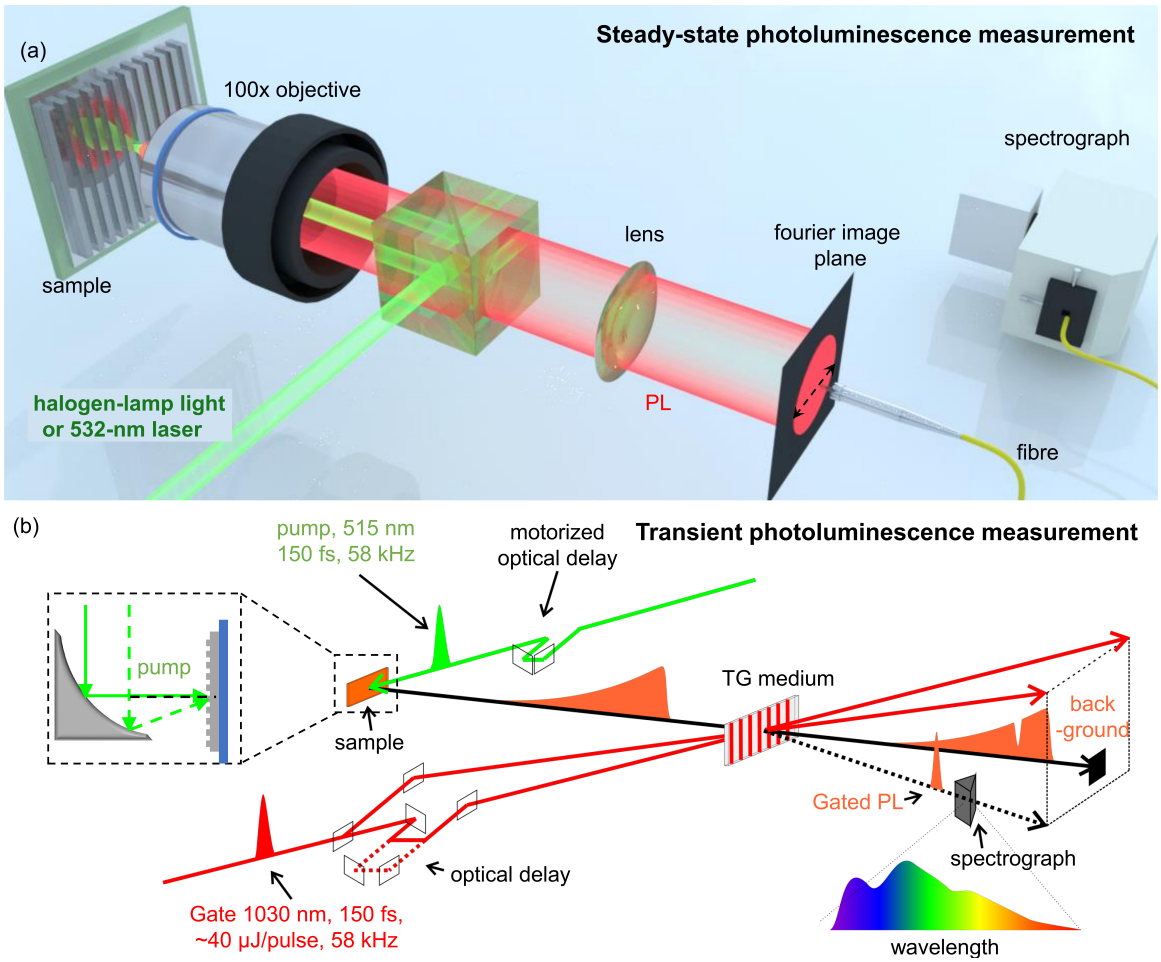

Fig. S 2. **Schematic of the measurement setup. a,** setup of angle-resolved steady-state PL (reflection). The samples are illuminated by a halogen lamp through a ×100 objective; and the reflected beam is analysed at the Fourier image plane to obtain angle-resolved data. **b,** setup of TPL measurements. The refractive index of the $\chi^{(3)}$ medium film can be periodically modulated by the interference of two control pulses at 1030 nm. The formed grating can be used to transiently diffract incoming light into the spectrograph.

A. Steady-state optical measurement

The angle resolved steady-state reflection and photoluminescence (PL) spectra were measured using the setup presented in Supplementary Fig. S2**a**. The samples are illuminated by a halogen lamp through a ×100 objective; and the reflected beam is collected through the same objective and then analysed at the Fourier image plane, which allows us to obtain the reflection spectra by using a fiber that is connected to a spectrometer (OceanOptics USB2000+VIS-NIR-ES) to scan the optical signals along the Fourier image plane. The fiber has a diameter 100 μm, enabling an angular resolution of 1°. Furthermore, a polarizer was installed before the detection plane to

analyse the polarization of the reflected beam. In steady-state PL measurements, the halogen lamp was replaced by a laser (532 nm and power 45 mW).

B. Transient optical measurement

The broadband transient PL (TPL) spectra have been measured using our transient grating PL spectrometer (Supplementary Fig. S2**b**)[4]. As the result of laser beam (1030 nm, $<$ 200 fs duration) interference on a silica film, the refractive index of the film can be periodically and transiently modulated, forming a refractive-index grating that can be used to transiently diffract incoming light. After pumping our samples with pulses (515 nm, $<$ 200 fs), the corresponding PL signals are collected and then projected onto the silica film. Varying the time difference between the PL signals and the transient refractive-index grating, we can get the broadband PL spectra at different time delays. This technique allows us to resolve the broadband PL with a time resolution of $\sim$ 100 fs. In addition, the spectral positions of TPL are calibrated with respect to the steady-state PL spectra. What's worth mentioning is that the TPL signals are collected from a wide angle range (-30° to 30°) to enhance the collection of PL signals, thus increasing the signal-to-noise ratio. Furthermore, we can exclude the possibility that directional LDOS enhancement results in the high-frequency feature observed in Fig. 3 of the manuscript, because the PL is collected from a wide angle range (Fig. S2**b** and Fig. S3**a**).

The angle-resolved transient absorption (TA) spectra were collected using the pump-probe method mentioned in ref [5], the pump pulse of which is same as what was used in the TPL measurements. The angle and polarization of both pump and probe beams can be flexibly adjusted to make the pump on- or off-resonant with the plasmons.

C. On/Off-resonance pump

The pump angle in the TPL measurements can be flexibly adjusted using the method shown in the inset of Fig. S2**b**. Due to the dispersive nature of the plasmons, the resonance for the no-spacer hybrids at the pump frequency (515 nm or 2.41 eV) can only be excited at $\theta = 23^\circ$ (Fig. S4) by p-polarized illumination (electric field parallel to x-z plane, see Fig. S3**a**). This means that pumping the QD-resonator hybrid at different angles or polarizations enables selective excitation of the plasmon that is on- or off-resonance with the pump.

Fig. S3**a** displays the TPL spectra of the no-spacer QD-resonator hybrid, with the pump being on-resonant or off-resonant with the plasmon modes. Specifically, we used p-polarized pump

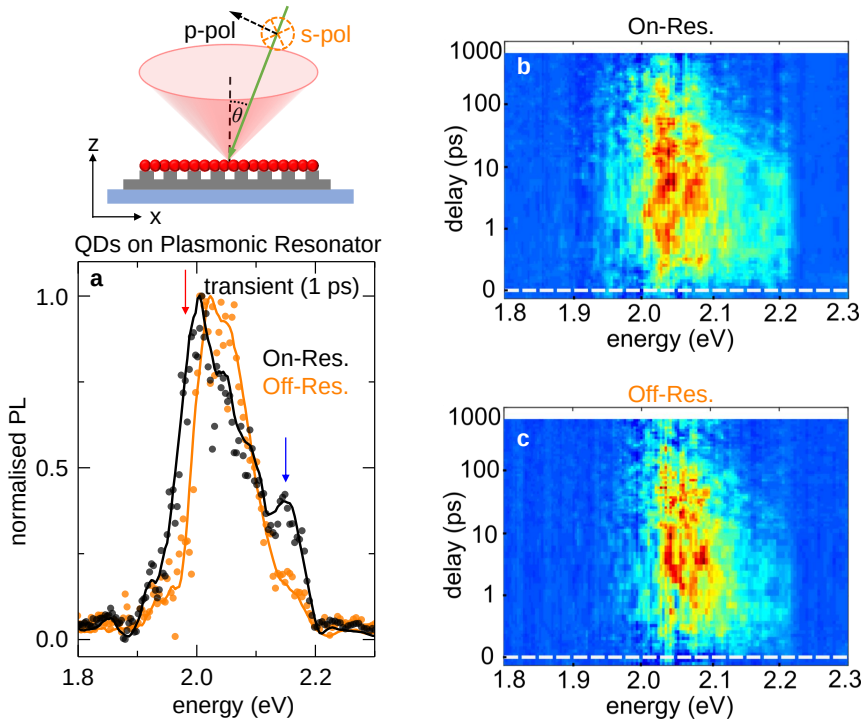

Fig. S 3. **Transient photoluminescence of the no-spacer QD-resonator hybrid for on/off-resonance pumping.** **a**, normalised PL transient at $t = 1$ ps from the hybrid excited by the pump that is (On-Res) or not (Off-Res) plasmonically enhanced, with the top schematic showing transient PL configuration, in which solid circles represent the measured transients, solid curves are the smoothed results. **b,** on-resonance measurement with a p-polarized pump with an incident angle of $\theta = 23°$. Emission at 2.15 eV can be easily identified. **c,** off-resonance measurement under a pump with an incident angle of $\theta = 37°$. Comparatively narrow emission is observed. The white horizontal dashed line indicates the arrival of the pump pulse $t = 0$. The data are normalized to individual maximum from 0 (blue) to 1 (red). The pump fluence was $25.6\,\mu\mathrm{J\,cm^{-2}}$.

at $\theta = 23°$ to resonantly enhance the pump (on-resonance) and change the polarization state to s-polarized (electric field perpendicular to x-z plane) to make the pump off-resonant with the plasmons. It turns out that the on-resonance excitation (black curve) broadens the PL transient ($t = 1$ ps after pumping), exhibiting an additional maximum at ~ 2.15 eV compared to the off-resonance transient (yellow curve) that only shows a peak at ~ 2 eV corresponding to the QD's bandedge transition $1S_e \rightarrow 1S_{3/2}$.

As previously mentioned, the transient TPL spectra of the no-spacer hybrids are also affected by the pumping angles. When the pump is less resonant, for example, incident angle is changed from $\theta = 23°$ to $37°$, the high-frequency TPL broadening becomes comparatively narrow, as depicted in Fig. S3**b** and S3**c**.

III. DISPERSIVE OPTICAL PROPERTIES OF THE PLASMONIC RESONATOR

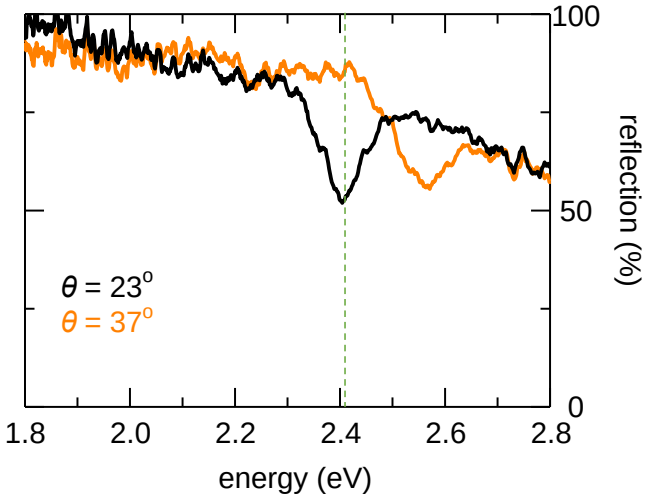

Fig. S 4. **Steady-state reflection spectra** under p-polarized illumination on the no-spacer QD-resonator hybrid at the incident angles of $\theta = 23°$ (black) and 37° (orange), respectively. The green dashed vertical line indicates the pump frequency in the TPL measurement in Fig. 3 in the main text, which matches the plasmon resonance excited at 23°.

The spectra presented in Fig. S4 show that when the no-spacer hybrid is exposed to p-polarized illumination at an incident angle of $\theta = 37°$, there is a dip in the reflection spectrum at 2.57 eV, indicating the absorption of photons at this frequency due to plasmon excitation. However, at a lower illumination angle of $\theta = 23°$, the plasmon resonance shifts towards longer wavelengths, causing the minimum in the reflection spectrum to shift to 2.41 eV, which corresponds to the frequency of the pump used in the transient optical measurements.

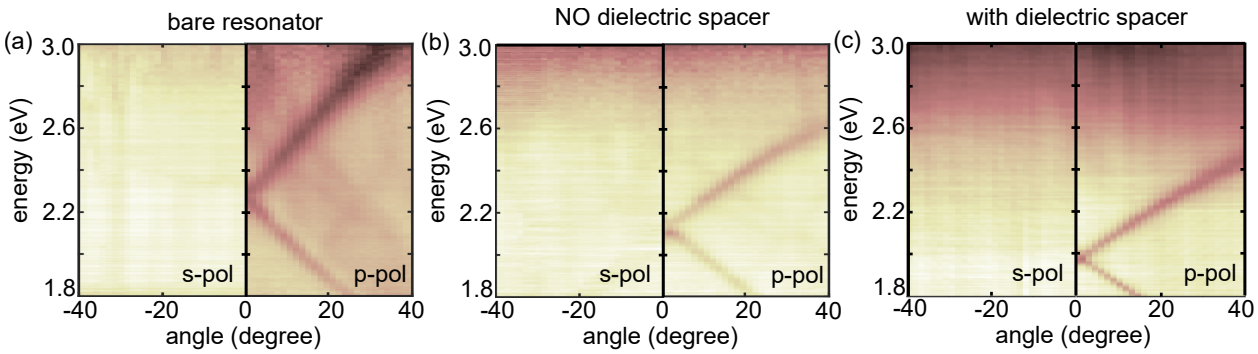

Fig. S 5. **Angle-resolved reflection spectra under s-polarized (left half) and p-polarized (right half) illuminations. a,** dispersion of our bare plasmonic resonator sample. **b,** dispersion of the no-spacer QD-resonator hybrid sample. **c,** dispersion of the spacer-embedded QD-resonator hybrid sample. Here the data are receptively normalized to their maxima. Bright, reflection maxima; dark, reflection minima.

The reflection spectra of the bare plasmonic resonator, the no-spacer hybrid, and the spacer-embedded hybrid are presented in Fig. S5 over a wide range of incident angles (0-40°). The reflection spectra under s-polarized illumination show no distinctive features, as plasmon resonances are not excited. On the other hand, when the illumination is p-polarized, the lattice plasmon resonances are excited at specific wavelengths and incident angles, which can be described by the equation $\frac{2n\cdot\pi\sin\theta}{\lambda} \pm \frac{2\pi}{\Lambda} = k_{\mathrm{spp}}$, where n is the reflective index of the coated material, Λ is the period of the metallic grating, and k_{spp} is the wave vector of surface plasmon.

These resonances are characterized by reflection minima in the spectra, as illustrated in Fig. S4, indicating that the resonator can easily absorb optical energy at these frequencies through plasmon excitation. Notably, the plasmon resonances in the hybrids, regardless of whether they are no-spacer or spacer-embedded, are usually red-shifted compared to those in the bare Ag resonator. This frequency shift is attributed to the refractive index change induced by the coated QD layer and the dielectric spacer. With the dispersion maps presented in Fig. S5, the plasmon resonance in our experiments can be set on or off resonance by adjusting the pumping angle or the pump polarization (refer to Fig. S2**b** and S3).

IV. DETERMINE THE RESONANT ENHANCEMENT OF ABSORPTION

To evaluate the absorption enhancement in the QD-resonator hybrids, we have conducted both numerical simulations (as illustrated in Fig. 3**a** and 3**b** in the main text) and experimental measurements, including steady-state photoluminescence and radiative lifetime measurements. These experiments reveal that the no-spacer hybrid exhibits an absorption enhancement of ~ 3. Here, we describe the outcomes of these two types of measurements, which are consistent with each other.

A. Plasmon enhanced Photoluminescence

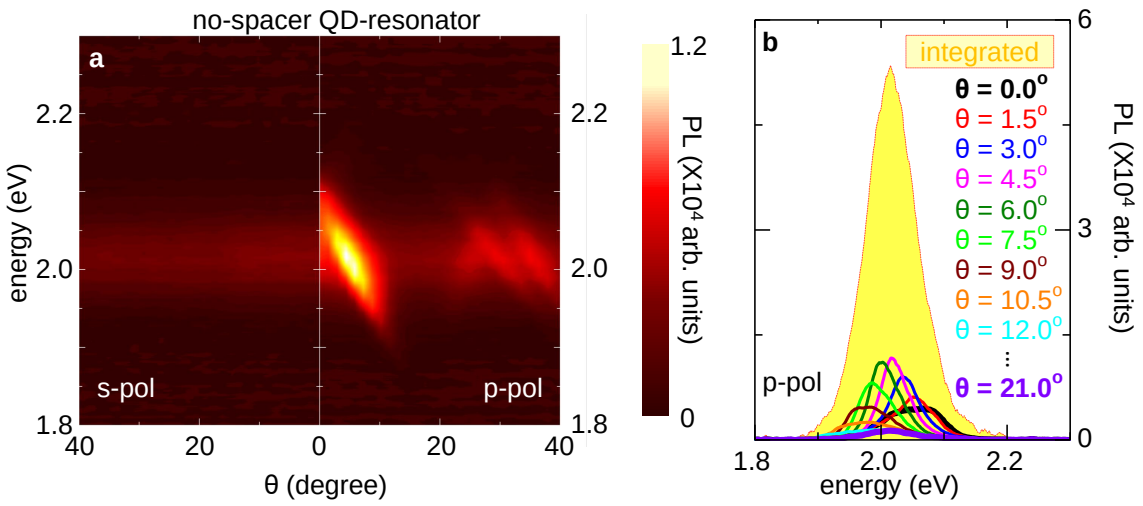

Fig. S 6. **Angle-Resolved steady-state Photoluminescence spectra** of the no-spacer QD-resonator hybrid with on-resonance pumping, presented in a form of **a,** an intensity plot as a function of both angle and frequency, with the left-half showing s-polarized spectra and right-half showing p-polarized spectra, and of **b,** PL spectra measured at angles θ_{probe} from 0° to 21°. Yellew area, the integrated PL intensity of all the stated angles.

In the main text, Fig. 3**a** displays a spatial map of $F_{\mathbf{P}}$, which is the ratio of $\gamma_{\mathbf{res}}$ to $\gamma_{\mathbf{0}}$ at the pump frequency $E = 2.41$ eV, where $\gamma_{\mathbf{res}}$ and $\gamma_{\mathbf{0}}$ respectively indicate the spontaneous emission rate of a dipole coupled to a plasmon resonance and the rate of a dipole in free space. This map represents the variation of local density of optical states (LDOS) for an emitter coupled to a plasmon. It is noteworthy that the plasmons in the grating-like structure can diffractively alter the LDOS, causing resonances to be excited at different incident angles (Fig. S4). Additionally, since the plasmon dispersion covers the spectral range of both absorption and emission of the QDs, the plasmon resonance can affect the absorption of the QDs to the pump together with the quantum yield of emission in a dispersive manner.

The impact of plasmon resonance on the emission of the QDs can be observed through the angle-resolved PL spectra. As illustrated in Fig. S6**a**, the PL spectra of the QD-resonator hybrids without a dielectric spacer are shown as a function of frequency and emission angles. The left panel shows s-polarized emission, which has a spectral peak centred around ~2.00 eV, the same as the emission of bare QDs, indicating no dispersion. In contrast, the p-polarized emission spectra on the right panel exhibit significant dispersive emission that is consistent with the plasmon resonances as depicted in Fig. S5**b**. Furthermore, it is noteworthy that under the same pump power, p-polarized emission generally displays much higher magnitudes than s-polarized emission.

In order to determine the total PL enhancement, it is necessary to remove the directional dependence of the emission. This is achieved by integrating the PL intensity over a wide range of angles (0°-21°) that covers the entire QD emission band. Fig. S6**b** illustrates this integration process for the p-polarized emission. The solid curves represent the p-polarized PL measured at various angles, while the yellow area indicates the integrated value.

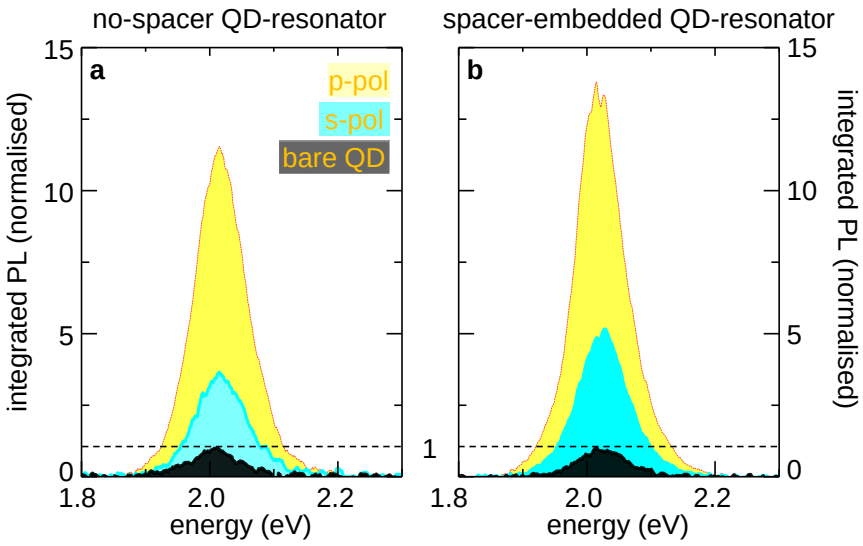

Fig. S 7. **Steady-state Photoluminescence.** The integrated PL intensity of the bare QD sample and the no-spacer and spacer-embedded hybrids with s- and p-polarized emission are compared in **a** and **b**, respectively. All spectra presented here are normalized to the peak value of the bare QD's PL to demonstrate enhancement. In all steady-state PL measurements, the pump laser frequency is 2.33 eV (532 nm) with p-polarization, and the laser beam is focused to a spot of diameter ~80 μm^2. Note that the PL emission of bare QDs is not polarization-dependent, so only the p-polarized emission is shown in this figure.

Fig. S7**a** demonstrates that the QD-resonator hybrid without a spacer (yellow area) can boost steady-state PL emission by around 12 times compared to the PL of the bare QD (black area). (It should be noted that all spectra presented in Fig. S7**a** are normalized to the peak value of the bare

QD's PL.) In this scenario, both the excitation and emission are p-polarized, indicating that both the QD's absorption of the pump and the QD's PL quantum yield are plasmonically enhanced.

However, if only p-polarized light is used to excite the hybrid and only s-polarized emission is collected (blue area in Fig. S7**a**), a much weaker PL enhancement of approximately 3.3 is observed. In this case, only the QD's absorption of the pump is enhanced by the plasmon resonance. In other words, the difference between the s-polarized emission in Fig. S7a and the emission from the bare QD is induced by the absorption enhancement, i.e. $F_{\mathbf{P}} \approx 3.3$.

The spacer-embedded hybrid, illustrated in Fig. S7b, exhibits a slightly higher but comparable PL enhancement to the no-spacer hybrid. Given that the LDOS enhancements in both structures are similar, as shown in Fig. 3**a** and 3**b** of the main text, the increased PL enhancement observed in the spacer-embedded sample may be attributed to either an increase in the quality factor of the resonator that includes the dielectric spacer or a lower occurrence of Auger-type recombination in the non-plasmonically doped QDs. Regardless of the specific mechanisms, the inclusion of the dielectric spacer results in an estimated five-fold increase in pump absorption in the spacer-embedded hybrid. Remarkably, despite the spacer-embedded sample having a higher absorption rate, it does not exhibit any high-frequency peaks in either the transient PL or absorption spectra, as seen in Fig. 3**e** and 3**k** of the main text, respectively. This finding confirms that the state-filling effect observed in the no-spacer hybrid is not caused by absorption enhancement.

B. Radiative lifetime

One can also estimate the change in LDOS by comparing the radiative lifetimes of quantum QDs with and without plasmonic enhancement. Placing QDs on a plasmonic resonator can result in a reduction in their radiative lifetime due to resonance enhancement at emission frequencies. To determine the enhancement of LDOS, we compared the radiative lifetime of a thin-film sample of bare QDs with that of a QD-resonator hybrid without a spacer. However, due to limitations in our TPL setup, we could not measure PL transients beyond 1000 ps. Therefore, we used TA spectroscopy to analyze the relaxations after 1000 ps, which corresponds to the process of QD's radiative emission [5].

Based on the TA measurements, we found that the radiative lifetime of bare QDs was 9.6 ns, which was consistent with a previous publication[2]. For the QD-resonator hybrid sample without a spacer, TA signals were measured for the bandedge emission at different pump intensities, as shown in Fig. S8. The fitted radiative lifetimes were 3.0, 2.8, and 2.4 ns for the three pumps,

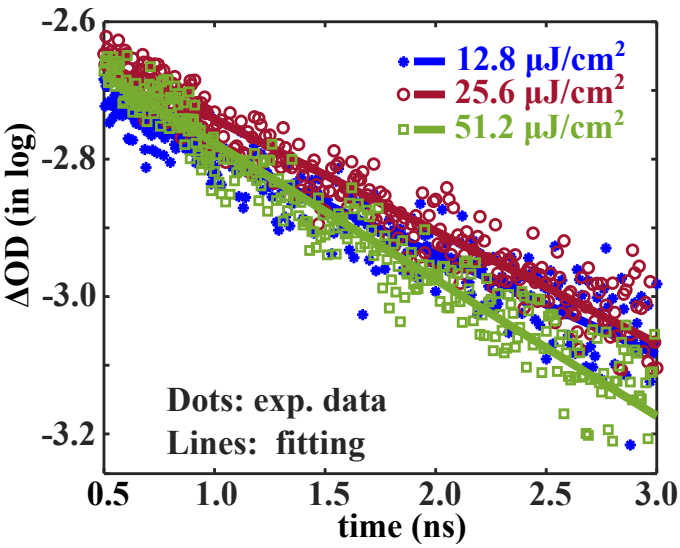

Fig. S 8. **Transient absorption signal for the QD-resonator hybrid sample.** Blue stars, experimental data of 12.8 μJ cm^{-2} pump; darkred circles, that of 25.6 μJ cm^{-2} pump; green squares, that of 51.2 μJ cm^{-2} pump. Solid lines are the corresponding fitted results.

respectively, indicating that the LDOS enhancement was approximately 3.2 at the emission frequency, which was consistent with steady-state measurements in Fig. S7.

It is important to note that the modification of LDOS at all plasmon frequencies exhibited similar magnitudes and spatial distributions. This suggests that although the dispersive plasmon modes are spectrally separated, they overlap spatially and can enhance both the pump absorption and quantum yield of PL emission at comparable levels. Thus, we can use $F_{\mathbf{P}} \approx 3.3$ as the factor of enhancement for the pump absorption in the QD-resonator hybrids.

V. TRANSIENT PHOTOLUMINESCENCE AT DIFFERENT PUMP POWERS

A. Data reproducibility

The TPL transients at specific time delays (τ = 5, 10, and 50 ps) presented in Fig. 3 of the main text provide a glimpse of the data. Nevertheless, the high-frequency feature is observable across a range of time delays and pump intensities. In Fig S9, we exhibit TPL measurements of the bare QDs and the QDs-resonator hybrid at different pump fluences to explicitly demonstrate the reproducibility of the broadened TPL of the no-spacer QD-resonator hybrid.

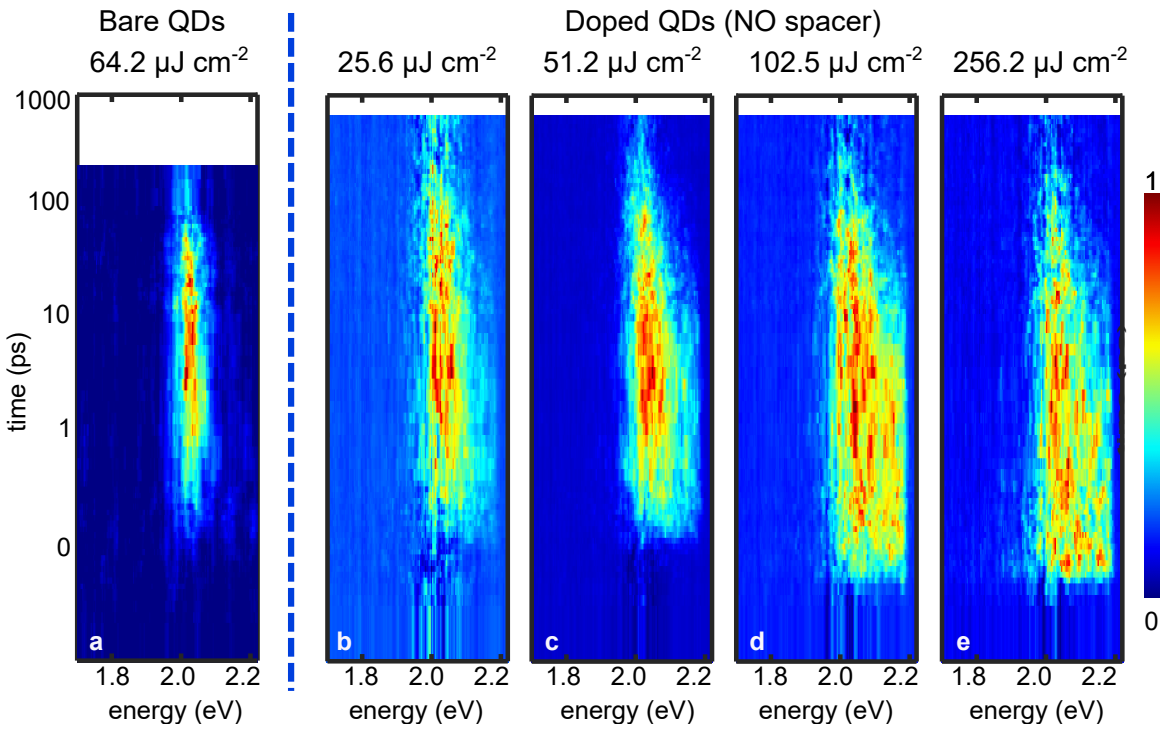

Fig. S 9. **TPL measurements at different pump fluences; a,** TPL of QDs on quartz with pump fluence of 64.19 μJ cm^{-2}. The right-hand side illustrated the TPL spectra of the doped QDs in the no-spacer QD-resonator hybrid with pump fluences of **b,** 25.6 **c,** 51.2 **d,** 102.4 and **e,** 256.2 μJ cm^{-2}. For all the surface plots, the intensity value is normalized from 0 (blue) to 1 (red).

Fig. S9**a** displays the TPL spectra of the bare QD sample with a pump fluence of 64.19 μJ cm^{-2}, showing a single peak at around 2.00 eV. For comparison, Fig. S9**b-e** exhibit the TPL spectra of the QDs-resonator hybrid without a dielectric spacer with pump fluences of 25.62 μJ/cm^2, 51.2 μJ/cm^2, 102.4 μJ/cm^2, and 256.2 μJ/cm^2. All three plots reveal a high-frequency emission feature at 2.15 eV that persists for tens of picoseconds after the pump pulse arrives.

B. Pump-dependent TPL

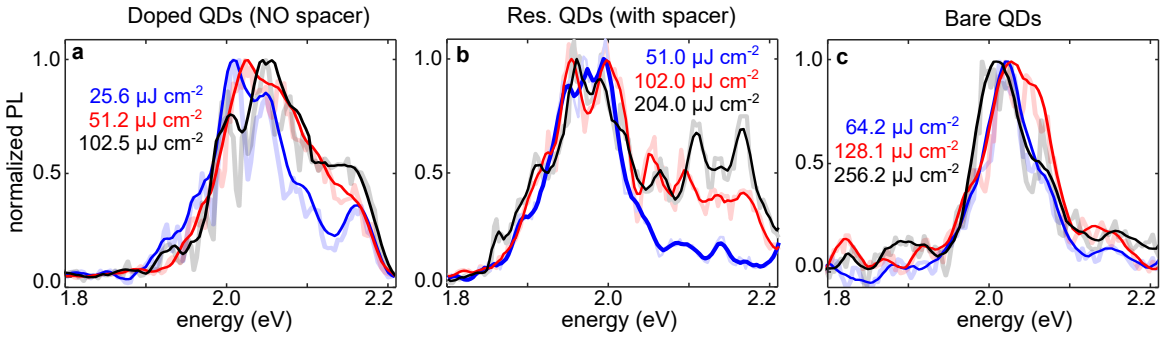

Fig. S 10. **Pump-dependent TPL measurements of different samples;** **a,** TPL spectra of the no-spacer QD-resonator hybrid with pump fluences as noted. **b,** TPL spectra of the spacer-embedded QD-resonator hybrid with pump fluences as noted. **c,** TPL spectra of the bare-QD sample with pump fluences as noted. For all the plots, the intensity value is normalized from 0 to 1.

Consistent with the main text, the spontaneous emission of high-energy states in the conduction band gives rise to the high-frequency emission. Under high pump power, the high-frequency feature is expected to manifest in all three samples: the doped QDs, the resonantly-enhanced QDs, and the bare QDs.

Figure S10 depicts the pump-dependent TPL of the three samples at a time delay of $\tau = 5$ ps. The high-frequency feature is apparent at pump fluences as low as 25.6 μJ/cm^2 for the doped QDs, whereas for the resonantly-enhanced QDs, which acquires greater absorption enhancement, the high-frequency emission does not emerge until the pump fluence reaches 102.0 μJ/cm^2. In contrast, in the bare QD sample, no broadened emission emerges until the pump is increased to 464.9 μJ/cm^2.

C. Pump-dependent TA

The TA spectra of QD-resonator hybrids without and with spacers at different pump fluences are presented in Fig. S11. For the doped QDs in the no-spacer hybrid, the spectra show a high-frequency bleaching at approximately 2.2 eV, which is easily noticeable even at a low pump fluence of 2.1 μJ/cm^2 (Fig. S11**a**). Consistent with the observation in TPL spectra, this feature emerges earlier than the main bleaching feature at approximately 2 eV , regardless of the pump fluences (Fig. S11**b**).

In contrast, the resonantly-enhanced QDs in the spacer-embedded hybrid exhibits a faint high-frequency feature only at a very high pump fluence of 101 μJ/cm^2 (Fig. S11**c**), which is 50 times

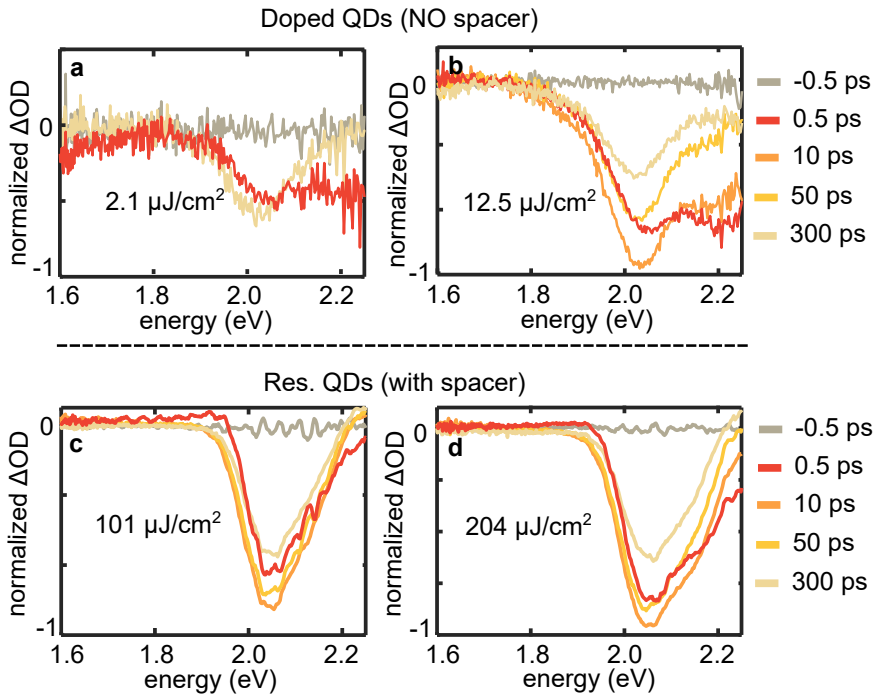

Fig. S 11. **Pump dependent TA measurements.** **a** and **b** TA spectra of the no-spacer QD-resonator hybrid with pump fluences as noted. **c** and **d** TA spectra of the spacer-embedded QD-resonator hybrid with pump fluences as noted. Normalized TA data are plotted for the sake of clarity.

stronger than the fluence required to trigger the 2.2 eV bleaching in the no-spacer hybrid. Although at a doubled pump fluence of 204 μJ/cm^2, the 2.2 eV bleaching feature becomes more noticeable, its amplitude remains weaker in the spacer-embedded hybrid than in the no-spacer one (Fig. S11**d**). The significant difference in the pump power that is required to generate the 2.2 eV bleaching indicates that the two systems are subject to different dynamical processes. The no-spacer hybrid can not be considered as an platform that simply enhances the optical absorption, and what plays a role is the plasmonic doping of hot electrons, which can lead to very high population with low excitations.

VI. TRANSITION ASSIGNMENT

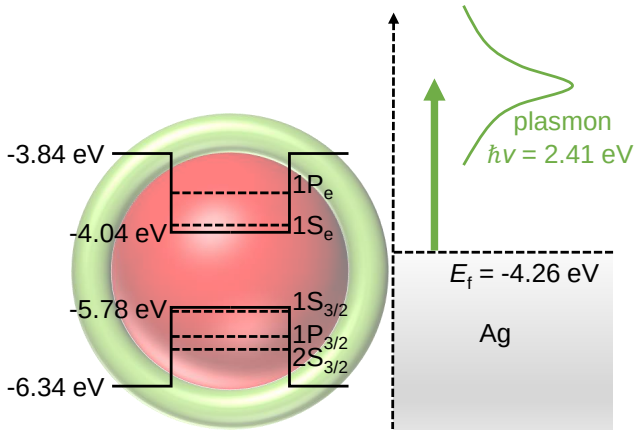

Fig. S 12. **Energy level diagram for the QDs coupled with Ag plasmonic resonator without a dielectric spacer.** The values of energy bands for CdSe/CdS (core/shell) QDs and fermi-energy of Ag are approximated from literature[5, 6]. The green curve indicates the excitation of plasmon in Ag resonator upon absorption of incident photons from TPL pump with frequency 2.41 eV.

The assignment of the TPL peaks of the no-spacer QD-resonator hybrid is critical in analysing the dynamics of excited electrons and holes. To compliment relevant discussions in the main text, here we provide more details. The energy band diagram of CdSe/CdS (core/shell) QDs and that of Ag metal are illustrated in Fig. S12. The transition frequencies of $1S_e - 1S_{3/2}$, $1P_e - 1P_{3/2}$ and $1S_e - 2S_{3/2}$ can also be found in our published paper [2]. The bandgap of QDs can be calculated using

$$E_{\mathrm{np}} = E_{\mathrm{g}} + \frac{h^2}{8\pi^2 r^2}[\frac{1}{m_e^*} + \frac{1}{m_h^*}] - \frac{1.8e^2}{4\pi\epsilon} \tag{S1}$$

where E_{np} is the bandgap energy of QDs, $E_g = 1.7$ eV is the bandgap of bulky CdSe, $h = 6.626 \times 10^{34}$ J/s is Planck constant, $e = 1.6 \times 10^{-19}$C is the charge of electron, $\epsilon = 9.57\epsilon_0$ is the dielectric constant of QDs, $m_e^* = m_e m_0$ and $m_h^* = m_h m_0$ with $m_e = 0.12$ and $m_h = 0.8$ are the effective masses of electron and hole respectively, and $m_0 = 9.1 \times 10^{-31}$ kg is the mass of an electron.

With the equation above we can easily assign the emission around 2.00 eV in Fig. S9 to the bandedge transition $1S_e - 1S_{3/2}$. The $1S_e - 1S_{3/2}$ emission in the no-spacer hybrid can be the mixture of single-exciton emission (one electron in $1S_e$ and one hole in $1S_{3/2}$) and charged-exciton emission (two electron in $1S_e$ and one hole in $1S_{3/2}$), where the electron-electron interaction can give rise to a spectral shift.

Besides the two aforementioned peaks around 2.00 eV in the no-spacer hybrid (Fig. 3**d** in the

main text), there exists an emission with high frequency at 2.15 eV. Because the energy structure inside a QD is discrete, to assign the 2.15 eV emission, we just need to involve the electronic states $1P_e$ and $1S_e$, and the hole states $S_{3/2}$, $1P_{3/2}$ and $2S_{3/2}$. Any other states are simply not relevant due to their too-high energies. Therefore there are six possible combinations. However, the possibilities of $1S_e - 2S_{3/2}$, $1P_e - 1P_{3/2}$ and $1P_e - 2S_{3/2}$ transition can easily be ruled out also because of the mismatch in transition frequencies. The possibility for $1S_e - 1P_{3/2}$ and $1S_e - 2S_{3/2}$ can be also excluded by considering the hole dynamics. As mentioned in the main text, photon emission from QDs naturally involving an electron and a hole. To activate the $1S_e - 1P_{3/2}$ and $1S_e - 2S_{3/2}$ transitions, the $1S_{3/2}$ and $1P_{3/2}$ hole states should be fully-filled in advance, which means that at least 5 and 9 holes, respectively, are needed in a single QD. Such numbers are far-beyond the optical absorption in our case (less than one exciton per QD).

With all these possibilities ruled out, the remaining $1P_e - 1S_{3/2}$ transition is responsible for the high-frequency emission of the no-spacer QD-resonator hybrid. Such a transition is usually forbidden, but the injection of hot electrons makes the QDs highly charged and breaks the selection rule for the electronic transitions. As a result, the usually forbidden $1P_e - 1S_{3/2}$ transition becomes allowed [7].

VII. ESTIMATION OF EXCITED CARRIERS

A. Estimating the excited carriers

The number of how many carriers are excited in individual QDs (excited carrier density N_{ex}) can be estimated with the equation:

$$N_{\mathrm{ex}} = \frac{F_{\mathrm{pump}} \cdot \sigma_{\mathrm{QD}}}{\hbar\omega} * F_{\mathrm{P}} \tag{S2}$$

where F_{pump} is the pump fluence, σ_{QD} is the absorption cross section of QDs, and F_{P} is the Purcell enhancement for the resonant laser pump. The σ_{QD} can be estimated from the steady-state absorption spectrum of the bare QD sample. This leads to an average excitation of $N_{\mathrm{ex}} \approx 0.16$ for each QD under the pump fluence of $25.62\,\mu\mathrm{J\,cm^{-2}}$, far below the theoretical excitation threshold ($N_{\mathrm{ex}} > 2$) for the $1P_{\mathrm{e}}$ state occupations. Taking $F_{\mathrm{P}} = 3.3$, we have $N_{\mathrm{ex}} = 0.56$ for $25.16\,\mu\mathrm{J\,cm^{-2}}$ pump, which means that even with the Purcell enhancement considered, the $1\mathrm{P_e} - 1\mathrm{S}_{3/2}$ transition still can not be triggered.

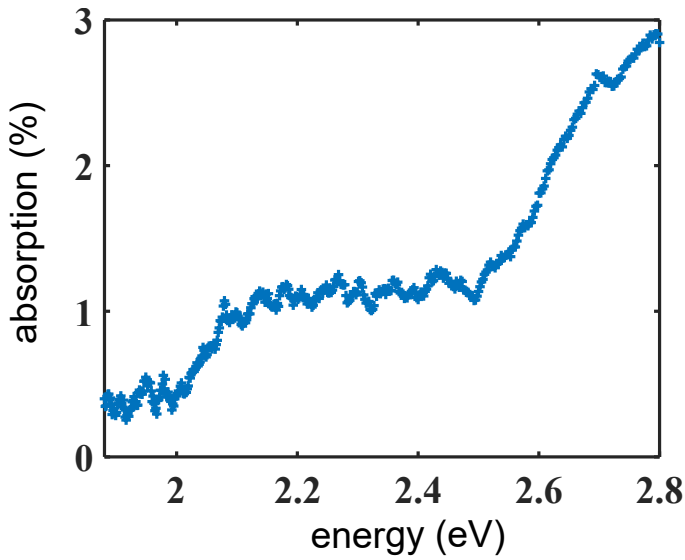

Fig. S 13. **Steady-state absorption spectrum of the bare QD sample.** The absorption magnitudes are obtained using the equation $A = 100\% - T - R - A_{\mathrm{glass}}$, where T and R stand for the transmission and reflection spectrum, respectively, measured on the bare QD sample, see Fig. S1**c**, and A_{glass} is the absorption of the glass substrate. The scattering of QDs is not included due to its low magnitude.

Note that the precise measurement of σ_{QD} can be challenging. We can on the other hand use the reflection spectrum of the QD-resonator hybrid to estimate N_{ex}. Reflection measurement of the QD resonator hybrid in Fig. S4 shows that 25% of the energy was absorbed by the hybrid (either

by the resonator or the QDs). If no hot electron doping is considered, the excitations per QD under the 25.62 μJ cm^{-2} pump (assuming QDs are closely packed) can be estimated using [11, 12]:

$$N_{\mathrm{ex}} = \frac{F_{\mathrm{pump}} \cdot A \cdot \pi r^2}{\hbar\omega \cdot T/d} \tag{S3}$$

where F_{pump} is the pump fluence, A is the absorption coefficient, r is the radios of QDs, $\hbar\omega$ is the energy of plasmon, T is the thickness of the QD layer, and d is the diameter of QDs. The AFM measurements of QD layer (Fig. S1c) advise a thickness of 45 nm (a stack of $\sim$ 7 QD layers). Even if all the optical energy that enters the hybrid (25%) is absorbed by the QDs (no light absorbed by the resonator at all, which is highly impossible), according to Eq. (S2), the number of electron per QD that each pump pulse can excite is $N_{\mathrm{ex}} = 0.9$, which is again not enough to generate the $1\mathrm{P_e} - 1\mathrm{S}_{3/2}$ transition. In fact, the actual absorption of QDs is much less than 25% as most of the optical energy is absorbed by the metallic resonator. Shown in Fig. S13 is the absorption spectra of our bare-QD thin film sample. The absorption at the pump frequency 2.41 eV is measured to be just $\sim 1\%$. For the photon emissions from CdSe/CdS QDs, Achermann et al [7] observed a broad PL signal from the $1\mathrm{P_e}$ level at a pump fluence of 3.4 mJ cm^{-2}, which correspond to $N_{\mathrm{ex}} \approx 10$. Similar results have been found by Bonati et al [8] and Fisher et al [9], where they reported observations of broad spectral features at a pump fluence of 10 mJ cm^{-2}. Our reference measurement (Fig. S10**c**) of bare QD thin film shows a noticeable $1\mathrm{P_e} - 1\mathrm{S}_{3/2}$ emission at 460 μJ cm^{-2} pump. Hence, the 2.15 eV emission at a low pump fluence of 25μJ cm^{-2} in our experiments can not be attributed to the enhancement of the pump absorption.

VIII. HOT ELECTRONS IN PLASMONIC RESONATORS

A. Multiple Hot-electron Generation

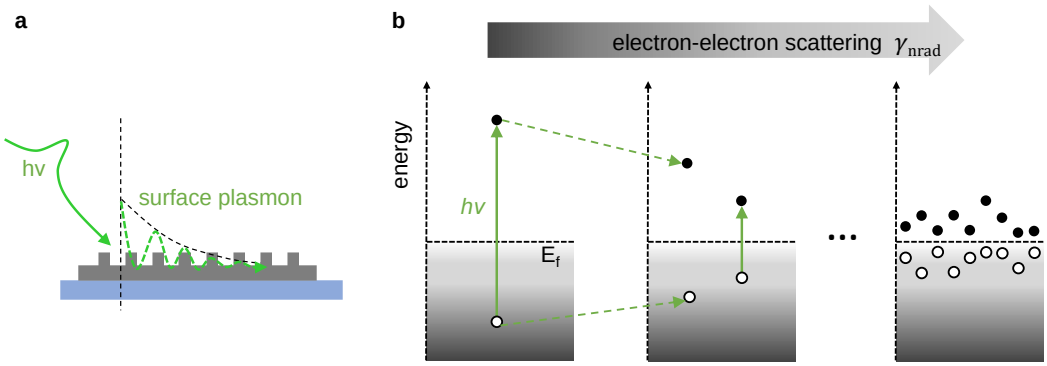

Fig. S 14. **Multiple Hot-electron Generation**. **a**, An input photon can generate a surface plasmon in a plasmonic resonator. **b**: Left, through nonradiative decay, a surface plasmon can elevate an electron to a new energy level of $h\nu$ higher than its initial. Middle, through electron-electron scattering, the energetic electron can collide with other electrons, losing a part of its energy and elevating another one. Right, as the electron-electron scattering continues, more and more secondary hot electrons are generated.

It is important to note that the decay of a single plasmon can lead to the generation of multiple hot electrons. As illustrated in Fig. S14, following coherent excitation, the energy of an excited surface plasmon can be approximately $h\nu$ higher than the Fermi level, where ν represents the plasmon frequency. These plasmons decay through collisions with electrons, causing the electrons to become highly energized. The energetic electrons can then collide with other electrons, transferring some of their energy and elevating their energy levels. For practical purposes, electrons with energy greater than an energy barrier ϕ_b are considered to be hot and useful, such as those higher than the Schottky barrier in a solar cell. In many cases, ϕ_b is much smaller than $h\nu$, meaning that secondary electrons produced by electron-electron scattering can still pass through the ϕ_b barrier. Therefore, even if only one plasmon is excited, the number of hot electrons n can be significant.

B. Decay of Hot Electrons

When plasmonic resonators are illuminated with light that resonates with their conduction-band electrons, it causes the excitation of collective oscillations of electrons called surface plasmons. The decay of surface plasmons occurs through three distinct processes, each with its own mathematical time constant [10]. These processes include: (a) Relaxation from a coherent excitation to a quasi-equilibrium electron distribution by means of electron-electron scattering, which oc-

curs within 0−100 fs. The electrons in the quasi-equilibrium distribution are hot electrons that can spread away because they possess energy higher than their Fermi level. (b) Cooling of hot-electrons by electron-phonon scattering that takes place from 1-10 ps, which can lead to a local lattice temperature rise. (c) Heat dissipation to the entire lattice or the environment via phonon-phonon scattering, which occurs over 100 ps.

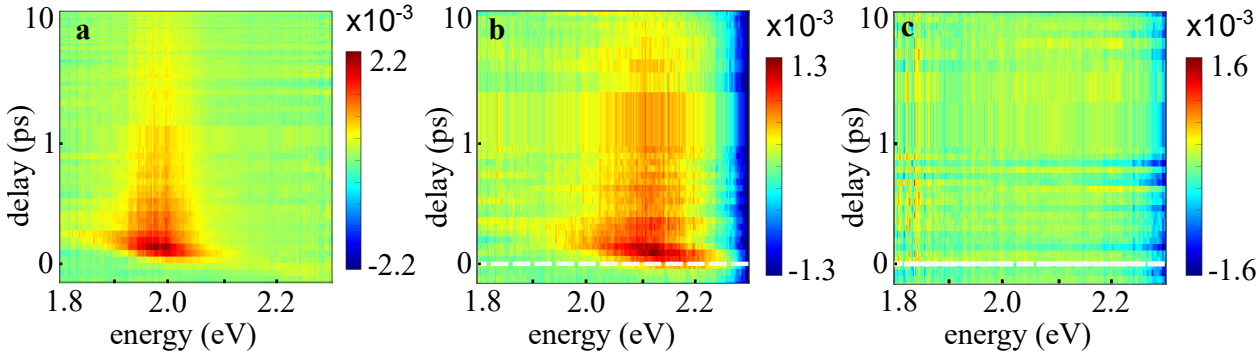

Fig. S 15. **Transient absorption spectra for the plasmonic resonator. a,** resonantly pumping at $\theta_{\text{pump}} = 6°$, and probing at $\theta_{\text{probe}} = 14°$. Hot electrons signal emerges at ≈ 2.0 eV. **b,** $\theta_{\text{probe}} = 8°$. Transient absorption maximum is blue-shift to 2.1 eV. **c,** off-resonant pumping $\theta_{\text{pump}} = 25°$, and probing at $\theta_{\text{probe}} = 20°$ shows no hot-electron signal. Here the pump fluence is 102.5 μJ cm^{-2}.

We have verified the time-dependent behavior of surface plasmons in our plasmonic resonator (without QDs) within the first 10 ps through TA measurements (Fig. S15). To match the corresponding plasmon resonances, we adjusted the pump (θ_{pump}) and probe (θ_{probe}) angles flexibly during the experiments. For this purpose, we employed a pump laser with a wavelength of 515 nm and an incident angle of $\theta_{\text{pump}} = 6°$ to excite the plasmon resonance at 2.41 eV (see Fig. S5**a**). Within the first 100 fs after excitation, surface plasmons decayed rapidly and generated a quasi-equilibrium electron distribution. In principle, these hot electrons can be detected in all directions that fall within the range of plasmon dispersion (Fig. S5**a**). When we probed the system at $\theta_{\text{probe}} = 14°$ (Fig. S15**a**), a red-shifted maximum was observed in the TA spectra compared to those probed at $\theta_{\text{probe}} = 8°$ (Fig. S15**b**), which agrees with the plasmon dispersion shown in Fig. S5**a**. However, when we off-resonantly excited the pump at $\theta_{\text{pump}} = 25°$, no hot-electron signal (Fig. S15**c**) was detected due to the weak excitation of surface plasmons.

C. Calculation of Hot Electron Density

Taking into account hot-electron generation from the metal Fermi gas, the number of excited electrons per QD can be significant. In the main text, the difference between resonance enhance-

ment and plasmonic doping is highlighted by the number of excited electrons. Without plasmonic doping, only one electron can be excited by absorbing one photon since carrier multiplication does not occur in our system when $\hbar\omega < 2E_g$, where E_g is the QD bandgap. However, absorbing one plasmon can produce multiple hot electrons, some of which may have energy higher than the barrier, and can dope the QDs, leading to the occupation of not only the $1P_e$ level but even higher levels. The number of hot electrons per QD can be estimated using the equation in [5],

$$N_{e^-} = \frac{F_{\text{pump}}}{2c\epsilon_0} \cdot |E/E_0|^2 \cdot \frac{8}{\pi^2} \frac{e^2 E_F^2}{\hbar} \frac{\hbar\omega - \Delta\phi_{TB}}{(\hbar\omega)^4} \cdot S_c \tag{S4}$$

where N_{e^-} represents the number of hot electrons per QD. The equation includes several parameters, such as the pump fluence F_{pump}, electron charge e, speed of light c, vacuum permittivity ϵ_0, light frequency ω, Ag Fermi-level E_F, tunneling barrier for electrons $\Delta\phi_{TB}$, calculated field enhancement $|E/E_0|^2$, and the contacting surface S_c between the QD and metal surface. Assuming S_c is 1 nm^2 and applying the field enhancement corresponding to Fig. 3**a** in the main text, we can estimate that N_e is equal to 32 for F_{pump} =25.16 μJ cm^{-2}.

The hot electron number, as shown in Equation (S4), exhibits a non-monotonic dependence on pump photon energy (ω). When a plasmon decays, it generates energetic electrons that rapidly thermalize to a local equilibrium according to Fermi-Dirac statistics, before they interacts with the lattice. At lower pump photon energies (ω), these energetic electrons do not possess enough energy to overcome the barrier for doping the QDs. However, at higher values of ω, the generation of hot electrons decreases due to intra-band transitions.

IX. MODIFIED EMISSION VIA PLASMONIC DOPING

A. Doping and relaxation

Fig. S16 provides an illustration of how plasmonic doping modifies the dynamics of spontaneous emission of QDs. When a pump laser is resonant with the plasmonic mode, it excites collective oscillation of electrons in the form of surface plasmons. Simultaneously, there is a possibility of generating an electron-hole pair in a QD, as depicted in Fig. S16a. The excited surface plasmons dephase within tens of femtoseconds, leading to the generation of multiple hot electrons, as demonstrated in Fig. S14 and Fig. S16b. Since these hot electrons have high energy, they can quickly fill the empty electron states in QDs and subsequently cool down. Once the holes in QDs relax to the bandedge, the spontaneous emission between $1P_e - 1S_{3/2}$ is immediately activated, as shown in Fig. S16c. As depicted in Fig. S17**a**, this cooling process of electron-hole pairs in QDs takes place on a sub-picosecond timescale.

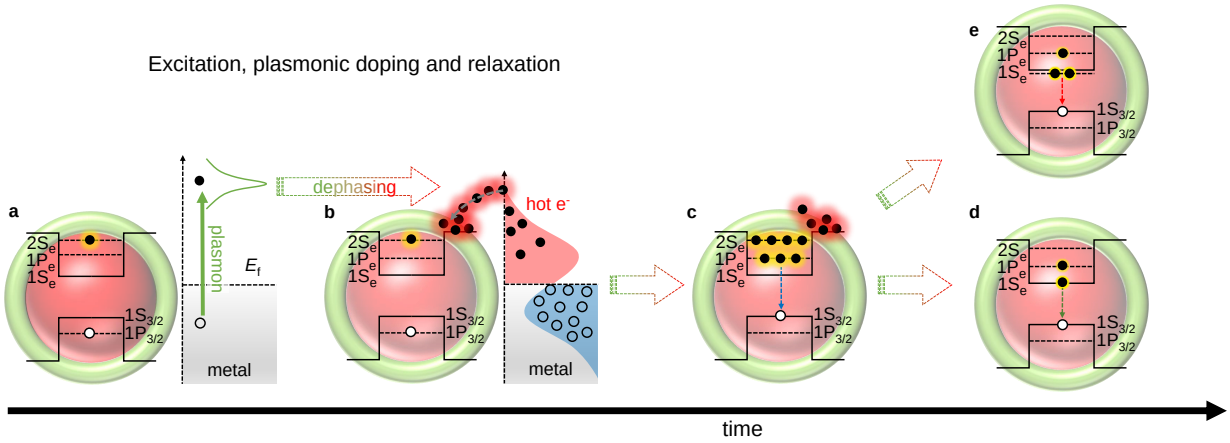

Fig. S 16. **Spontaneous emission modified by plasmonic doping**. **a**, when the pump laser is on resonance with the plasmonic mode, surface plasmons can be excited in the metallic resonator; meanwhile an electron-hole pair may be excited in an adjacent QD. **b**, surface plasmons generate multiple hot electrons within tens of femtoseconds. **c**, the doping of hot electrons and the cooling of electron-hole pairs in QDs all take place within sub-picoseconds. Therefore the $1P_e - 1S_{3/2}$ transition reaches its maximum within less than one picosecond. The decay of multiple hot electrons results in two relaxation senarios: **d**, one electron or **e**, two electrons in the $1S_e$ state, correpsonding to Fig. S17**c**.

It should be noted that the transfer of hot electrons from the metal surface to the QDs is dependent on the contact between them. Hence, the hot electron decay process in the QDs may be non-uniform, depending on the specific details of the doping process. For QDs that are lightly doped or undoped, hot electrons decay via Auger recombination, resulting in one hole and one

electron remaining in the bandedge, which enables the 2.05 eV spontaneous emission (Fig. S16d and Fig. S17**b**). In contrast, for heavily doped QDs, the 1S state may be fully occupied by two electrons, with residual electrons remaining in the 1P state. This enables the coexistence of the 2.15 eV $1P_e - 1S_{3/2}$ transition and the 1.99 eV $1S_e - 1S_{3/2}$ emission (as the energy is lowered due to the occupation of two electrons in the 1S state), which is consistent with the measurements in Fig. S17 and Fig. 4 of the main text. As the pump fluence increases, more electrons enter the QDs, causing the spontaneous emission at the bandedge to be dominated by the 1.99 eV emission rather than the 2.05 eV emission. This observation agrees with the measurement in Fig. S9.

B. TPL decays

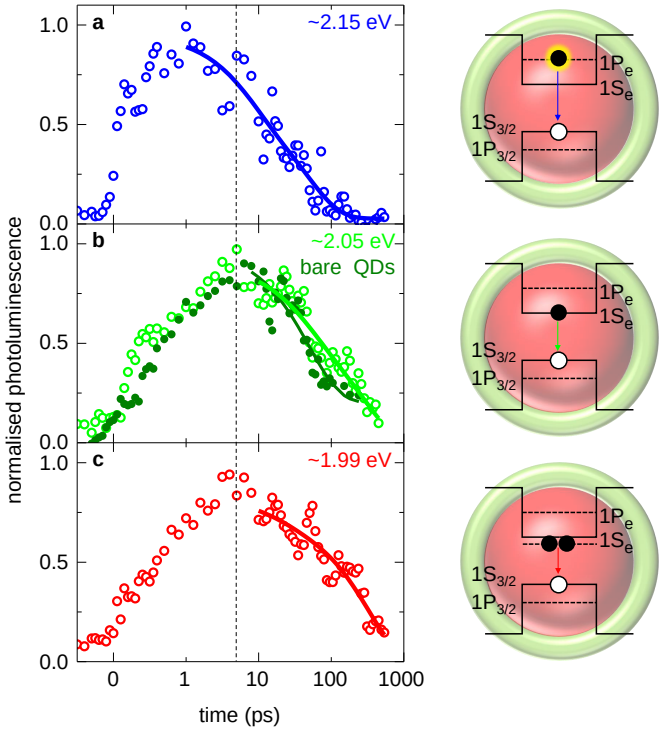

Fig. S 17. **Relaxations in QDs.** Normalised transient PL (open circles) as a function of time of the doped QDs at **a**, ~ 2.15 eV, **b**, ~ 2.05 eV and **c**, ~ 1.99 eV, corresponding to the fitting maxima in Fig. 3**d** (main text); the bare QD decay is plotted (dark green solid circles) in panel **b**. The solid curves are the single- (panel **b** and **c**) or bi- (panel **a**) exponential fitted results with parameters demonstrated in Table S1, while the dotted vertical line indicates the time point where the bandedge emission achieves its maximum.

The time-dependent relaxations of the three primary TPL components from doped QDs are displayed in Fig. S17, and they correspond to the dashed curves in Fig. 3**d** of the main text. These

curves represent the fitting results obtained using a Gaussian function (Eq. S5):

$$\chi(\omega) = a + \sum_{j=1} b_j \cdot \frac{1}{\sqrt{2\pi}\sigma_j} \exp[-(\omega - \omega_j)^2/(2\sigma_j^2)] \tag{S5}$$

where ω_j and σ_j represent resonant frequency and width of peak respectively. The TPL signal of the doped QDs were then decomposed into three transitions with frequencies located at 1.99 eV, 2.05 eV and 2.15 eV, as highlighted by the dashed red, green and blue dashed curves in Fig. 3**d** in the main text.

The rapid increase in the 2.15 eV TPL signal (< 1 ps, Fig. S17a) implies that high-energy states in the QDs are already occupied at 1 ps. The slower band-edge signal maxima at approximately 8 ps (Figs. S17b, S17c) indicate it takes longer to populate lower-energy states. This temporal difference demonstrates a top-down injection process, where electrons enter the QDs at higher-energy stats, before relaxing to lower ones. This preferential high-to-low relaxation is consistent with the TA data (Fig. 3j). Furthermore, the resulting $1S_e$ level filling induces a bandgap reduction (Fig. S17c) and a red-shifted emission (1.99 eV), also reflected in TA bleaching.

Table. S I. **Decay dynamics of thin-film bare QDs films and doped QDs.** The two decay channels included in the fitting are fast non-radiative (τ_{fast}) decay and slow radiative (τ_{slow}) decays. Data shown in the table corresponds to the dashed curves in Fig. 3**d** and 3**f** in main text.

	Transitions (eV)	τ_{fast} (ps)*	τ_{slow} (ps) †
Bare QDs	2.05	73	~9.6×10^3
Doped QDs	1.99	285	~3.0×10^3
	2.05	101	~3.0×10^3
	2.15	27	128

* τ_{fast} takes into account the effect of, for example, electron-photon interactions;

† For the doped QDs, τ_{slow} at 2.05 and 1.99 eV are taken as the slow-process time in Fig. S8, and τ_{slow} at 2.15 eV is a obtained from fitting.

The TPL decay dynamics of the doped QDs were fitted using a biexponential model denoted as $F(t) = A\exp(-t/\tau_{\text{fast}}) + B\exp(-t/\tau_{\text{slow}}) + C$, as shown in Fig. S17 and listed in Table SI. For the 1.99 and 2.05 eV transitions, τ_{slow} is the radiative lifetime determined by TA measurements, resulting in a single-exponential model where we only need to determine τ_{fast}. We note that the $1P_e - 1S_{3/2}$ transition at 2.15 eV decays much faster than the two transitions at the QD bandedge. The transient PL spectrum of bare QDs is also included for comparison.

[1] Du, K., Wathuthanthri, I., Mao, W., Xu, W. & Choi, C.-H. Large-area pattern transfer of metallic nanostructures on glass substrates via interference lithography. *Nanotechnology* **22**, 285306 (2011).

[2] Bisschop, S., Geiregat, P., Aubert, T. & Hens, Z. The impact of core/shell sizes on the optical gain characteristics of cdse/cds quantum dots. *ACS Nano* **12**, 9011–9021 (2018).

[3] Cirillo, M. *et al.* "Flash" Synthesis of CdSe/CdS Core-Shell Quantum dots. *Chem. Mater.* **26**, 1154–1160 (2014).

[4] Chen, K., Gallaher, J. K., Barker, A. J. & Hodgkiss, J. M. Transient grating photoluminescence spectroscopy: an ultrafast method of gating broadband spectra. *J. Phys. Chem. Lett.* **5**, 1732–1737 (2014).

[5] Chen, Y.-H. *et al.* Bandgap control in two-dimensional semiconductors via coherent doping of plasmonic hot electrons. *Nat. Commun.* **12**, 4332 (2021). .

[6] Samokhvalov, P., Linkov, P., Michel, J., Molinari, M. & Nabiev, I. Photoluminescence quantum yield of cdse-zns/cds/zns core-multishell quantum dots approaches 100% due to enhancement of charge carrier confinement. In *Colloidal Nanoparticles for Biomedical Applications IX*, vol. 8955, 89550S (International Society for Optics and Photonics, 2014).

[7] Achermann, M., Hollingsworth, J. A. & Klimov, V. I. Multiexcitons confined within a subexcitonic volume: Spectroscopic and dynamical signatures of neutral and charged biexcitons in ultrasmall semiconductor nanocrystals. *Phys. Rev. B.* **68**, 245302 (2003).

[8] Bonati, C. *et al.* Spectral and dynamical characterization of multiexcitons in colloidal cdse semiconductor quantum dots. *Phys. Rev. B.* **71**, 205317 (2005).

[9] Fisher, B., Caruge, J. M., Zehnder, D. & Bawendi, M. Room-temperature ordered photon emission from multiexciton states in single cdse core-shell nanocrystals. *Phys. Rev. Lett.* **94**, 087403 (2005).

[10] Khurgin, J. B. Fundamental limits of hot carrier injection from metal in nanoplasmonics. *Nanophotonics* **9**, 453–471 (2020).

[11] Hu, F. *et al.* Superior optical properties of perovskite nanocrystals as single photon emitters. *ACS Nano* **9**, 12410–12416 (2015).

[12] Hu, F. *et al.* Carrier multiplication in a single semiconductor nanocrystal. *Phys. Rev. Lett.* **116**, 106404 (2016).